energies

MDPI

Article

Energy, Exergy, and Environmental Screening of Mechanical, Chemical, and Thermal Recycling Pathways for End-of-Life Crystalline Silicon Photovoltaic Modules: Implications for Recycling Infrastructure Planning and Decision Support

Min Young Kim [1] and Sung Joo Hong [2,*]

[1] Department of Public Administration, Jeonju University, Jeonju-si 55069, Jeonbuk, Republic of Korea
[2] Department of Mechanical and Automotive Engineering, Jeonju University, Jeonju-si 55069, Jeonbuk, Republic of Korea
* Correspondence: hongsz@jj.ac.kr

Abstract

The increasing deployment of crystalline silicon photovoltaic (c-Si PV) modules is expected to generate substantial end-of-life waste, requiring recycling strategies that consider material recovery, energy use, environmental performance, and future infrastructure needs. This study develops a literature-informed energy–exergy screening framework for comparing mechanical (MR), chemical (CR), and thermal recycling (TR) pathways. Literature-derived process evidence was distinguished from calculated indicators and scenario-based parameters to accommodate differences in process scale and data completeness. The literature inventory indicated 96.0 kWh t^{-1} of electricity for a pilot-scale MR process, while documented solvent/ultrasonic EVA delamination and pyrolysis required 7.14 and 25.0 kWh m^{-2}, respectively. Under the assumed reference scenario, energy demands were 1.72, 4.30, and 6.77 kWh $panel^{-1}$ for MR, CR, and TR, respectively, with corresponding scenario-based screening thermodynamic efficiency indicators of 48.4%, 50.9%, and 53.1%. The analysis identified mechanical liberation, EVA removal, and thermal decomposition as pathway-specific process hotspots. Integrated environmental and infrastructure scenarios further demonstrated that pathway relevance depends on waste throughput, facility scale, and electricity decarbonization. The framework therefore provides a transparent screening approach for linking heterogeneous process evidence with recycling-infrastructure planning and decision support, without prescribing a universally superior recycling pathway.

Keywords: circular economy; end-of-life photovoltaic modules; energy–exergy analysis; recycling infrastructure planning; thermodynamic screening

Check for updates

Academic Editor: Joshua M. Pearce

Received: 28 September 2026
Revised: 20 October 2026
Accepted: 23 October 2026
Published: 29 October 2026

Copyright: © 2026 by the authors. Licensee MDPI, Basel, Switzerland. This article is an open access article distributed under the terms and conditions of the Creative Commons Attribution (CC BY) license.

1. Introduction

The rapid deployment of photovoltaic (PV) technology has made solar electricity an increasingly important component of the global transition toward low-carbon energy systems. This expansion, however, is accompanied by a delayed but rapidly growing end-of-life (EoL) waste stream because PV modules have finite service lifetimes and may also be retired prematurely because of damage, degradation, or technological replacement. Crystalline silicon (c-Si) technology is of particular importance because of its dominant historical and current market position and, consequently, its expected contribution to future PV waste. EoL c-Si PV modules contain large quantities of glass and aluminum

together with silicon, copper, silver, polymers, and other materials whose recovery can reduce demand for primary resources and mitigate the environmental consequences of inappropriate disposal. Previous studies have therefore increasingly treated discarded PV modules not only as an emerging waste-management problem but also as a potential secondary resource within a circular economy [1–4].

The multilayer structure of c-Si PV modules nevertheless makes high-quality recycling technically challenging. Glass, silicon cells, metallic conductors, ethylene-vinyl acetate (EVA) encapsulant, polymeric backsheets, and aluminum frames are physically integrated into a durable laminated structure designed to resist separation during decades of outdoor operation. Recycling therefore generally requires combinations of dismantling, delamination, size reduction, physical separation, and subsequent material recovery or purification. Mechanical recycling (MR) relies primarily on comminution and physical separation and can provide comparatively simple processing of bulk materials, although liberation and recovery of high-value constituents may remain limited. Akimoto et al. (2018) demonstrated high-voltage pulse crushing and physical separation, highlighting the limitations of mechanical classification for precious-metal recovery [5]. More recent mechanical studies similarly emphasize that dedicated PV treatment can improve material liberation and product quality compared with conventional undifferentiated WEEE processing [6,7].

Chemical and thermal routes provide alternative mechanisms for overcoming the strong adhesion created by the encapsulant. Chemical recycling (CR) can employ acids or organic solvents to promote EVA dissolution or swelling and facilitate the separation of glass and solar cells. Kim and Lee (2012), for instance, demonstrated ultrasonic-assisted EVA treatment using organic solvents and showed that solvent type, temperature, ultrasonic power, and treatment time strongly influence delamination behavior [8]. Pagnanelli et al. (2019) subsequently investigated cyclohexane treatment following pilot-scale mechanical processing and demonstrated the potential for recovering high-grade glass from the coarse fraction of shredded PV modules [9]. Such routes, however, introduce additional requirements associated with solvent or reagent consumption, recovery, wastewater treatment, and process time. Thermal recycling (TR), in contrast, uses elevated temperatures to decompose polymeric encapsulation and facilitate material separation. Thermal treatment can effectively expose glass, cells, and metallic components, but its performance depends strongly on temperature, residence time, polymer composition, atmosphere, and off-gas management [1,10,11]. Dobra et al. (2022) demonstrated that thermal-delamination time depends strongly on treatment temperature and prior backsheet removal [10].

These technological differences create trade-offs that cannot be represented adequately by material-recovery rate alone. Recovery of a greater number of materials or achievement of higher-purity products may require additional electricity, heat, chemicals, or downstream treatment. Dias et al. (2016) reported Ag concentration yields of 94% for a milling–sieving–leaching route and 92% when pyrolysis was additionally introduced, indicating that the addition of an energy-intensive thermal step does not necessarily produce a corresponding improvement in the targeted recovery outcome [12]. Conversely, integrated processes can achieve high overall recycling and recovery rates when complementary operations are combined; Rubino et al. (2020), for example, reported an optimized process with an 82% recycling rate and an estimated 94% recovery rate [13]. These findings suggest that the assessment of PV recycling requires simultaneous consideration of process intensity, material-recovery objectives, and the quality of recovered products rather than the use of a single recovery metric.

Life-cycle assessment (LCA) has provided an important basis for evaluating these trade-offs. Comparative studies have shown that recycling can reduce environmental burdens through recovery of secondary materials, but the results depend substantially on

the recycling technology, chemicals and energy consumed, transportation, system boundaries, and credits assigned to avoided primary production. Lunardi et al. (2018) compared mechanical, thermal, and chemical recycling with other EoL options and highlighted both the environmental benefits of material recovery and the potential burdens associated with toxic substances and transportation [1]. Maani et al. (2020) further demonstrated that environmental impacts vary substantially among recycling methods and identified Ag, Al, Si, and glass as priority materials for c-Si recycling from an environmental and economic perspective [14]. Pilot-scale studies have also shown the importance of process-specific evidence. Del Pero et al. (2019), using predominantly primary data from a mobile mechanical recycling device, found that operational electricity consumption—particularly pre-treatment, milling, and separation—was a major contributor to environmental impacts [15]. Ansanelli et al. (2021) similarly identified energy consumption, chemicals, and transportation as important environmental hotspots in a pilot-scale c-Si PV recovery process [16].

Energy consumption alone, however, does not fully describe the thermodynamic implications of alternative recycling pathways. Electricity, low- or high-temperature heat, and chemical resources differ in their capacity to perform useful work, while material liberation and purification inevitably involve thermodynamic degradation. Exergy analysis provides a second-law perspective by accounting for these differences in energy quality and can therefore complement conventional energy and environmental indicators. This distinction is particularly relevant to PV recycling because mechanical operations are predominantly electricity-driven, thermal routes involve high-temperature energy requirements, and chemical routes may combine electricity with material-intensive solvent and reagent inputs. Jech et al. (2025) recently demonstrated the value of combining exergy analysis with LCA for silicon PV recycling, using HSC Chemistry simulations to compare incineration, pyrolysis, ultrasound-assisted solvent treatment, and mechanical recycling [17]. Their results showed that thermodynamic and environmental rankings need not coincide, reinforcing the need to evaluate recycling technologies using more than material recovery or energy demand alone.

A practical difficulty remains, however, when such comparative assessments are extended beyond a specific simulated process. Published PV-recycling data are heterogeneous in process scale, functional unit, system boundary, module composition, operating conditions, and reporting completeness. Some studies provide primary pilot-scale electricity inventories, whereas others report laboratory operating conditions, reagent consumption, material yields, or harmonized LCA inventories. Del Pero et al. (2019), for example, provide primary operational data for a pilot mechanical process [15], whereas chemical and thermal investigations frequently focus on specific delamination or recovery operations rather than complete industrial process inventories [8–10]. Dias et al. (2021) explicitly distinguished laboratory experimental performance from an optimized high-throughput process in their technical, environmental, and economic assessment, illustrating how strongly process scale can affect interpretation of recycling performance [3]. Consequently, assigning apparently precise industrial-scale values to every unit operation can create a level of certainty that is not supported by the available evidence.

This limitation becomes increasingly important when process assessment is connected to recycling-system planning. Future EoL PV management is not solely a question of identifying a technically efficient unit operation. The amount and spatial distribution of PV waste, facility throughput, economies of scale, transportation requirements, electricity supply, recovery targets, and timing of investment can all affect the practical suitability of recycling configurations. Del Pero et al. (2019) noted that mobile processing can reduce transport-related environmental burdens, illustrating how facility configuration

can alter the performance of a recycling system beyond the characteristics of individual unit operations [15]. Pagnanelli et al. (2019) similarly emphasized that expected waste collection constrains feasible plant scale and therefore affects economic assessment [9]. Recent reviews have similarly identified recycling infrastructure, process scalability, and regulatory implementation as important constraints on the transition toward large-scale PV recycling systems [18]. Recent reviews have also highlighted the technological, environmental, and implementation challenges associated with the growing volume of end-of-life PV modules [19]. From this perspective, recycling technology assessment becomes not only a process-engineering problem but also an infrastructure-planning and decision-support problem under technological and data uncertainty. This distinction is particularly relevant during the transition from laboratory and pilot technologies toward larger-scale PV recycling networks.

Despite these advances, three research gaps remain. First, existing recycling studies generally focus on individual processes or specific environmental and thermodynamic assessments, while differences in functional units, process boundaries, and technological maturity limit direct comparison across recycling pathways. Second, although previous studies have combined exergy and environmental analysis, a transparent distinction between literature-supported evidence, calculated indicators, and scenario-based assumptions remains important when equivalent industrial-scale inventories are unavailable. Third, the connection between process-level energy–environmental trade-offs and broader recycling-infrastructure conditions, including future waste throughput, facility scale, and electricity decarbonization, remains insufficiently explored within a common screening framework. Addressing these gaps motivated the present study, which integrates evidence classification, comparative process screening, and infrastructure-oriented scenario analysis without assuming that the available literature represents fully validated industrial recycling systems.

Accordingly, the present study develops a literature-informed energy–exergy screening framework for representative mechanical, chemical, and thermal recycling pathways for EoL c-Si PV modules. The framework is not intended to reproduce or predict the exact performance of a specific commercial recycling facility. Instead, it explicitly distinguishes the literature-supported evidence, calculated indicators, and scenario-based screening parameters, thereby preserving the provenance and limitations of heterogeneous process data. The analysis first compares stage-wise energy requirements and identifies process hotspots; it then applies thermodynamic screening to examine energy-quality and irreversibility-related trade-offs and integrates these indicators with environmental performance. The process-level assessment is subsequently extended to future waste generation, facility-scale effects, and electricity-decarbonization scenarios to examine how technology characteristics interact with recycling-infrastructure conditions. In this way, the study addresses four related objectives: (i) to establish a literature-informed basis for comparing the energy characteristics of MR, CR, and TR; (ii) to identify pathway-specific thermodynamic trade-offs and process hotspots within an explicitly screening-level framework; (iii) to examine the combined environmental–thermodynamic positioning of alternative pathways; and (iv) to explore how waste throughput, facility scale, and electricity decarbonization may influence process and infrastructure decision support. Rather than identifying a universally superior recycling technology, the framework is intended to reveal the conditions under which individual or hybrid pathways may become more appropriate for a developing EoL PV recycling system.

2. Methodology

2.1. System Boundary and Recycling Pathways

The present study evaluates three representative end-of-life (EoL) recycling pathways for crystalline silicon photovoltaic (c-Si PV) modules: mechanical recycling (MR), chemical recycling (CR), and thermal recycling (TR). These pathways are defined as screening archetypes assembled from representative process configurations reported in the literature, rather than as models of three specific commercial recycling plants. This distinction is necessary because the available literature differs substantially in process scale, module characteristics, functional unit, system boundary, and reporting completeness. Accordingly, the purpose of the comparison is to identify pathway-level energy, thermodynamic, and environmental trade-offs under a common screening framework, rather than to predict the exact performance of a particular industrial facility.

The core process boundary begins with the receipt of an EoL c-Si PV module at the recycling facility and includes the principal operations required for module dismantling, delamination or size reduction, material liberation, and physical or chemical separation. Upstream PV-module manufacturing and the operational phase of the PV system are excluded because the analysis focuses specifically on EoL treatment. Collection and long-distance transportation are also excluded from the core process comparison because they depend strongly on the spatial configuration of the recycling system rather than on the intrinsic characteristics of the recycling pathway. Where environmental benefits associated with recovered materials are considered, avoided primary-material production is treated separately as an environmental credit. Infrastructure-scale effects, future waste throughput, facility capacity, and electricity-decarbonization conditions are subsequently introduced as scenario variables in the infrastructure-level screening analysis rather than embedded in the core process inventory.

The mechanical recycling (MR) pathway represents processes in which material liberation is achieved predominantly through physical operations, including dismantling or pre-treatment, crushing or milling, and subsequent separation of glass, silicon-rich fractions, metals, and polymers. Mechanical processing is already used in PV and conventional WEEE treatment and generally involves fewer chemical inputs than solvent- or acid-based routes. However, physical liberation does not necessarily provide high recovery of all valuable constituents. For example, Akimoto et al. (2018) demonstrated that high-voltage pulse crushing combined with sieving and density separation could effectively separate major material fractions, while only 33.2% of the total Ag was concentrated in selected Ag-rich particle-size fractions, indicating the limitations of mechanical classification for complete precious-metal recovery [5]. For the energy screening in the present study, the MR archetype is primarily calibrated using the pilot-scale mechanical treatment investigated by Del Pero et al. (2019), whose inventory was based mainly on primary measurements from a mobile recycling device and resolved electricity consumption among pre-treatment and subsequent material-separation operations [15].

The chemical recycling (CR) pathway represents processes in which encapsulant removal and/or valuable-material recovery is promoted using organic solvents, acids, or other chemical reagents, with physical pre-treatment where required. Chemical delamination can facilitate separation of the laminated module structure at substantially lower temperatures than thermal decomposition. Kim and Lee (2012) demonstrated ultrasonic-assisted EVA treatment using organic solvents and showed that solvent type, temperature, ultrasonic power, and treatment duration strongly affect delamination behavior [8]. Pagnanelli et al. (2019) subsequently demonstrated solvent treatment using cyclohexane at 50 °C for 1 h on a coarse fraction obtained from pilot-scale mechanical treatment, enabling recovery of high-grade glass [9]. Chemical processing can also target valuable metals;

Dias et al. (2016), for example, investigated nitric-acid leaching for Ag concentration from mechanically treated c-Si PV modules [12]. In the present framework, CR therefore represents a mechanical-pre-treatment–delamination–chemical-recovery archetype, rather than a single fixed industrial flowsheet.

The thermal recycling (TR) pathway represents processes in which elevated temperature is used to degrade or remove EVA and other polymeric layers, thereby enabling subsequent separation of glass, silicon-cell material, and metallic components. Thermal treatment can provide effective delamination but introduces additional requirements associated with high-temperature energy supply and treatment of gaseous decomposition products, particularly when fluorinated backsheets are present. Fiandra et al. (2019) demonstrated that mechanical removal of polymeric layers followed by thermal treatment can reduce these environmental and operational problems and reported effective material separation at 500 °C under controlled treatment conditions [2]. Dobra et al. (2022) further demonstrated a clear temperature–residence-time relationship, with complete delamination requiring 65 min at 500 °C and 33 min at 600 °C; prior backsheet removal reduced treatment duration by more than 45% at each investigated temperature [10]. The TR archetype used here therefore encompasses thermal delamination or pyrolysis together with the subsequent separation and off-gas-management functions required by such processing, while the quantitative status of individual inputs is distinguished according to the evidence framework described in Section 2.2.

For harmonization of the literature-evidence layer, a mass-normalized basis of 1 tonne of EoL c-Si PV module feed was adopted where conversion was supported by the source data. Original literature values were retained in their reported units when conversion required unsupported assumptions. A separate nominal per-panel reference case was defined for scenario-based screening rather than as a measured module with specified mass, area, or material composition. Accordingly, literature-reported quantities were not directly converted into the stage-wise inputs of the reference scenario.

Figure 1 summarizes the resulting system boundary and the principal operations assigned to the three pathway archetypes. Although the pathways are displayed separately for comparative purposes, they should not be interpreted as mutually exclusive technological alternatives. Practical PV recycling systems may combine mechanical pre-treatment with subsequent chemical or thermal processing. Indeed, pilot and experimental studies have demonstrated the potential benefits of such integrated configurations, including mechanical treatment followed by solvent delamination and combined mechanical–thermal processing. Accordingly, MR, CR, and TR are used here as analytical archetypes to identify process-level trade-offs, while the implications of pathway combinations, facility scale, waste throughput, and energy-system conditions are considered subsequently within the decision-support framework.

2.2. The Literature-Informed Evidence and Parameter Classification

A literature-informed process inventory was developed to replace the illustrative inputs used in the preliminary screening model. The objective of the calibration was not to construct a synthetic industrial plant by combining all the available literature values, but to establish a transparent quantitative basis for comparing the representative recycling archetypes defined in Section 2.1. Priority was therefore given to original studies reporting experimental measurements, pilot-scale operating data, process inventories, or explicitly documented operating conditions for EoL c-Si PV recycling. Review articles and harmonized life-cycle inventories were used primarily where comparable primary process data were unavailable or where normalization across different recycling technologies was required.

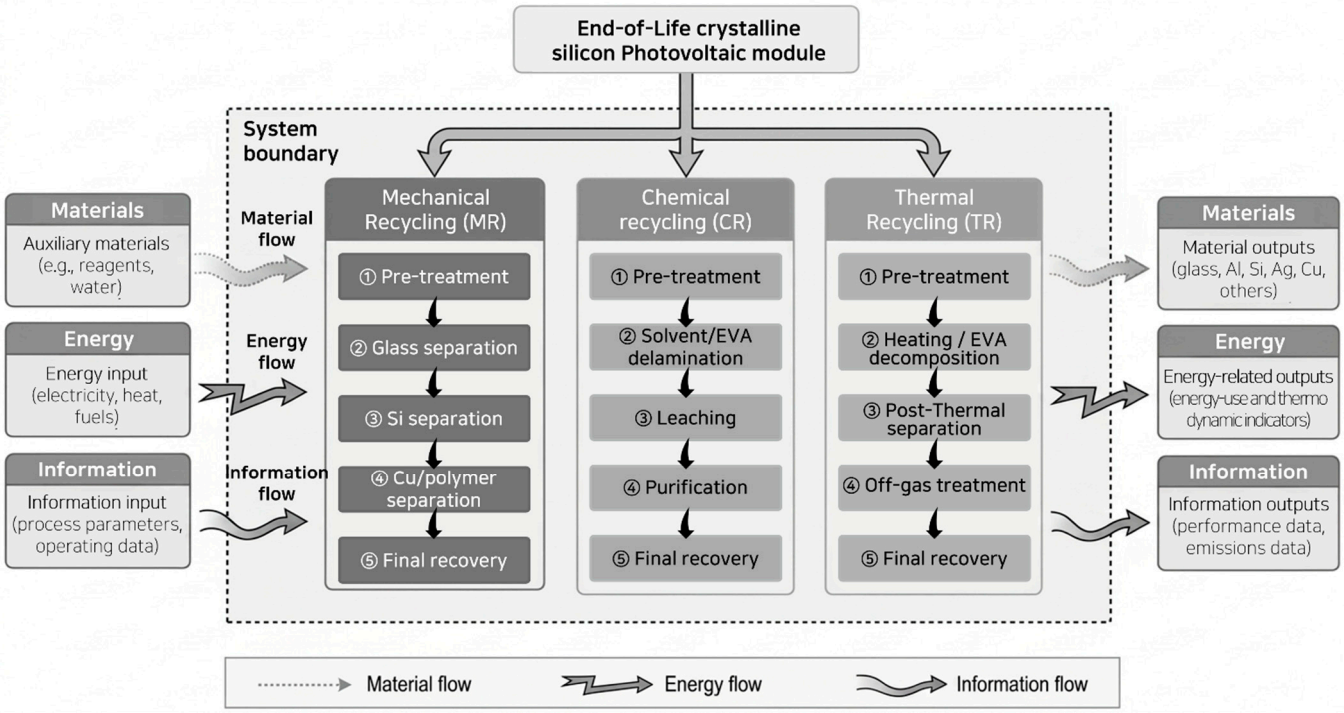


Figure 1. System boundary and representative process archetypes considered in the energy–exergy screening of EoL c-Si PV recycling. MR, CR, and TR denote mechanical, chemical, and thermal recycling, respectively.

The available evidence differs substantially in technological maturity and reporting basis. For mechanical recycling, Del Pero et al. (2019) reported a 20 kg PV panel as the functional unit and developed the life-cycle inventory mainly from primary data collected directly from a mobile recycling device [15]. Their analysis also resolved the operational contribution of pre-treatment and subsequent glass, silicon, copper, and polymer-fraction separation, providing a comparatively strong basis for stage-level calibration of the MR pathway. Chemical-treatment studies are more heterogeneous. Pagnanelli et al. (2019) combined pilot-scale mechanical treatment with solvent delamination of the coarse fraction using cyclohexane at 50 °C for 1 h [9], whereas Kim and Lee (2012) investigated ultrasonic-assisted EVA dissolution under controlled laboratory conditions using several organic solvents [8]. Dias et al. (2016) investigated nitric-acid leaching for silver recovery and explicitly compared routes with and without an additional pyrolysis step [12]. Thermal-treatment evidence similarly consists predominantly of controlled experimental studies. Fiandra et al. (2019) investigated polymer removal and material separation at 500 °C [2], while Dobra et al. (2022) quantified the relationship between treatment temperature, residence time, and mechanical backsheet pre-treatment over the range of 500–600 °C [10].

Because these studies do not constitute three directly equivalent industrial process inventories, the quantitative information used in the model was classified according to its epistemic status. Three categories were defined: evidence-based (E), calculated (C), and scenario-based (S). Evidence-based parameters are values reported directly in the underlying literature, including measured electricity consumption, reagent quantities, treatment temperatures, residence times, and material-recovery data. Calculated parameters are values obtained from evidence-based quantities through explicit unit conversions, normalization, or thermodynamic relationships without introducing an additional empirical assumption. Scenario-based parameters are quantities introduced only where the available literature does not provide sufficiently comparable industrial-scale evidence but where parametric exploration is required for thermodynamic or infrastructure-level screening.

Accordingly, the three categories are defined as follows:

$$X = \begin{cases} X^E, \text{ directly reported evidence} \\ f(X^E), \text{ calculated quantity } (X^c) \\ X^S, \text{ explicit screening-scenario parameter} \end{cases} \quad (1)$$

This classification prevents experimentally reported quantities from being presented with the same evidential status as model-derived or scenario-based quantities. In particular, an *S*-classified parameter is not interpreted as a measured industrial value, and results that depend on such a parameter are reported as screening or scenario outcomes rather than plant-performance predictions.

2.2.1. Normalization of the Literature Data

The literature employs different functional units, including energy per module, per unit mass, and per unit area. For comparison at the process level, convertible quantities were normalized to the common functional unit of 1 tonne of EoL c-Si PV module feed defined in Section 2.1. Where an energy requirement was originally reported on a mass basis, conversion was performed directly as follows:

$$E_t = E_m \times 1000 \quad (2)$$

Here, E_m is the specific energy requirement in kWh kg^{-1}, and E_t is the corresponding value in kWh t^{-1}.

For data reported per module, the following is established:

$$E_t = \frac{E_{\text{module}}}{m_{\text{module}}/1000} \quad (3)$$

Here, E_{module} is the reported energy consumption in kWh $module^{-1}$, and m_{module} is the corresponding module mass in kg. For example, the pilot-scale inventory of Del Pero et al. (2019) is based on treatment of a 20 kg PV panel, allowing direct conversion of the reported module-level electricity inputs to a mass-normalized basis [15].

For area-based data, conversion was performed only when the corresponding module mass-to-area ratio was available from the underlying inventory:

$$E_t = E_A \left(\frac{1000}{m_A} \right) \quad (4)$$

Here, E_A is the reported energy requirement in kWh m^{-2}, and m_A is the module mass intensity in kg m^{-2}. Maani et al. (2020), for example, adopted an area-based functional unit of 1 m^2 of PV panel waste for comparing recycling methods, illustrating the need for explicit normalization when combining such inventories with mass- or module-based process data [14].

The original values and units were retained in the literature-informed inventory before normalization. A conversion was performed only when all quantities required by Equations (2)–(4) were explicitly available or traceable to the same inventory basis. Where conversion would require an unsupported assumption regarding module mass, area, process throughput, or operating duration, the original literature value was retained and was not treated as directly comparable with normalized pathway totals.

2.2.2. Treatment of Scale and Incomplete Process Inventories

Process scale was retained as an explicit attribute of the literature evidence because laboratory-, pilot-, and industrial-scale process data were not assumed to be directly

interchangeable. This distinction is particularly important for PV recycling, for which many advanced delamination and material-recovery technologies remain at laboratory or pilot scale. Differences in throughput, equipment utilization, heat integration, solvent recovery, and auxiliary requirements can substantially affect the specific energy and environmental performance of a recycling process. Accordingly, the literature values were interpreted within their originally reported process scale and system boundary rather than treated as directly equivalent industrial inventories.

No numerical value was assigned to an unreported unit operation within the literature-evidence layer solely to complete a pathway inventory. Missing stage-level electricity, heat, reagent, operating-condition, or recovery data were therefore retained as not reported unless they could be derived transparently from directly reported quantities. Consequently, the evidence summarized in Table 1 does not necessarily represent complete and mutually equivalent process inventories for all three pathways. The mechanical inventory derived from Del Pero et al. (2019), for example, represents a documented multi-stage pilot-scale process, whereas several chemical and thermal studies quantify specific delamination, leaching, or thermal-treatment operations rather than complete commercial recycling pathways [15]. Table 1 should therefore be interpreted as a literature-informed evidence layer that establishes the empirical context, process conditions, and plausible magnitude of key recycling inputs, rather than as a directly harmonized dataset for calculating pathway-level performance.

Table 1. Literature-derived process evidence used to calibrate the energy–exergy screening framework for end-of-life c-Si PV module recycling.

Pathway	Stage	The Literature-Informed Process Input	Reported/ Normalized Value	Source
Mechanical recycling (MR)	Pre-treatment	Electricity	39.5 kWh t^{-1}	[15]
	Glass separation	Electricity	25.5 kWh t^{-1}	[15]
	Si separation	Electricity	23.0 kWh t^{-1}	[15]
	Cu/polymer separation	Electricity	8.0 kWh t^{-1}	[15]
	MR total	Electricity	96.0 kWh t^{-1}	[15]
Chemical recycling (CR)	EVA delamination	Solvent + ultrasonic irradiation	7.14 kWh m^{-2}	[14]
	EVA delamination	o-DCB solvent	46.2 kg m^{-2}	[14]
	Alternative solvent delamination	Cyclohexane; 50 °C; 1 h; S/L = 0.2 g mL^{-1}; stirring	—	[9]
	Chemical treatment	HNO_3/HF/CH_3COOH/Br_2	5208/3125/3125/ 62.5 mL m^{-2}	[14]
	Ag leaching	64% HNO_3; 5 g solid/100 mL; 2 h; room temperature	—	[12]
Thermal recycling (TR)	Pyrolysis/EVA decomposition	Electricity	25.0 kWh m^{-2}	[14]
	Thermal delamination	500/550/600 °C	—	[10]
	Residence time	65/47/33 min at 500/550/600 °C	—	[10]
	Oxidative thermal treatment	500 °C, 60 min	—	[2]

NOTE: The original literature units were retained unless conversion to the common functional basis could be performed without additional assumptions.

Because complete stage-resolved inventories under equivalent system boundaries were unavailable for MR, CR, and TR, a separate reference-case screening dataset was defined for comparative analysis, as summarized in Table 2. The energy inputs and irreversibility coefficients in Table 2 were prescribed as exploratory scenario parameters rather than derived through direct normalization or empirical calibration of Table 1. Their purpose is to examine assumed stage-level differences under a consistent computational framework. These parameters are classified as scenario-based (*S*) quantities and are not interpreted as experimentally measured industrial inventories or directly measured exergy-destruction fractions. Their purpose is to provide a transparent and reproducible reference scenario through which relative pathway behavior, stage-level thermodynamic hotspots, and sensitivity to alternative irreversibility assumptions can be examined.

Table 2. Reference-case parameters used for scenario-based energy–exergy screening.

Pathway	Stage	Energy Input [kWh/Panel]	Scenario-Based Irreversibility Coefficient, φ^S
Mechanical recycling (MR)	Pre-treatment	0.71	0.15
	Crushing and milling	0.87	0.85
	Sieving/separation	0.14	0.30
MR total		1.72	-
Chemical recycling (CR)	Pre-treatment	0.55	0.15
	EVA removal	1.43	0.75
	Leaching	1.04	0.55
	Purification	1.28	0.30
CR total		4.30	-
Thermal recycling (TR)	Pre-treatment	0.40	0.15
	Heating/EVA decomposition	4.50	0.55
	Post-thermal separation	0.11	0.20
	Off-gas treatment	1.76	0.35
TR total		6.77	-

NOTE: The reference-case parameters are screening variables and should not be interpreted as measured industrial process inventories. The energy inputs define a common comparative scenario informed by and interpreted against the literature evidence summarized in Table 1. The coefficient φ^S is a dimensionless scenario-based irreversibility parameter rather than a directly measured exergy-destruction fraction. Supplementary Table S1 summarizes the evidence classification, provenance, and computational roles of the principal model parameters and derived indicators. Calculated outputs that depend on scenario-based inputs are explicitly distinguished from the independently reported literature evidence.

The two datasets therefore serve distinct but complementary purposes. Table 1 describes what is quantitatively supported by the published recycling literature, whereas Table 2 defines the common reference scenario used for pathway-level energy–exergy screening. Literature evidence is used to contextualize and assess the physical plausibility of the screening results, while calculations based on Table 2 are explicitly reported as reference-case or scenario-based outcomes rather than predictions of commercial-plant performance. This separation prevents heterogeneous literature measurements and model assumptions from being assigned the same evidential status and enables incomplete process evidence to inform, rather than artificially complete, the comparative screening framework.

2.3. Energy–Exergy Screening Analysis

The process-level assessment was conducted in two complementary layers. First, the reference-case energy demand of each recycling pathway was quantified from the stage-wise scenario inputs defined in Table 2. Second, an exergy-informed thermodynamic screening was performed to examine how alternative assumptions regarding stage-specific irreversibility affect the relative thermodynamic behavior of the three pathway archetypes. The latter is intended as a screening analysis rather than a complete process exergy balance, because equivalent measurements of physical and chemical exergy entering and leaving every unit operation are not available for all three pathways.

For each pathway p, the total reference-case energy demand was calculated as the sum of the stage-wise energy inputs:

$$E_p^S = \sum_{i=1}^{n_p} E_{p,i}^S \tag{5}$$

Here, ${E_p}^S$ is the total reference-case energy demand of pathway p [kWh panel^{-1}], ${E_{p,i}}^S$ is the energy input assigned to process stage i, and n_p is the number of stages included in the pathway archetype. The superscript S indicates that these values belong to the reference screening scenario defined in Table 2 and should not be interpreted as measured industrial energy inventories.

The contribution of each process stage to the total pathway energy demand was calculated as follows:

$$C_{e,p,i} = \frac{E_{p,i}^S}{E_p^S} \times 100 \tag{6}$$

Here, $C_{E,p,i}$ is the percentage contribution of stage i to the total reference-case energy demand of pathway p. This stage-wise decomposition was used to identify the relative concentration of energy requirements within each recycling pathway.

Because complete stage-resolved input–output exergy inventories are unavailable for equivalent MR, CR, and TR systems, plant-specific exergy destruction was not calculated. Instead, a dimensionless scenario-based irreversibility coefficient, φ^S, was assigned to each reference-case process stage, as summarized in Table 2. The stage-wise screening irreversibility indicator was defined as follows:

$$I_{p,i}^{scr} = \varphi_{p,i}^S E_{p,i}^S \tag{7}$$

The pathway-level value was obtained as follows:

$$I_p^{scr} = \sum_{i=1}^{n_p} I_{p,i}^{scr} \tag{8}$$

Here, ${I_{p,i}}^{scr}$ and ${I_p}^{scr}$ denote the stage-level and pathway-level screening irreversibility indicators, respectively; ${E_{p,i}}^S$ is the reference-case stage energy input; and φ^S is the corresponding scenario-based coefficient.

For comparative evaluation, the screening thermodynamic efficiency was defined as follows:

$$\eta_{th,p}^{scr} = \left(1 - \frac{I_p^{scr}}{E_p^S}\right) \times 100 \tag{9}$$

Here, ${\varphi_{p,i}}^S$ represents a prescribed stage-specific scenario weight rather than an experimentally measured or physically derived exergy-destruction fraction. The selected values reflect assumed differences in stage-level loss intensity and are not independently calibrated against measured exergy balances. Accordingly, the resulting irreversibility indicators and

screening thermodynamic efficiencies should not be interpreted as actual exergy destruction or conventional second-law efficiencies. Chemical exergy associated with solvents and reagents in CR is excluded because comparable stage-resolved inventories are unavailable. For TR, the heat-exergy factor $\psi_Q = 1 - T_0/T$, where T_0 = 298.15 K, is evaluated separately to illustrate the quality of supplied heat and is not incorporated into the principal screening efficiency calculation.

2.4. Environmental–Thermodynamic Screening Indicators

To integrate environmental and thermodynamic performance within a common screening framework, three pathway-level indicators were considered: net global warming potential (GWP) benefit, screening thermodynamic efficiency, and total reference-case energy demand. The net GWP benefit of pathway p was defined as follows:

$$B^S_{\mathrm{GWP},p} = \mathrm{GWP}^S_{\mathrm{avoided},p} - \mathrm{GWP}^S_{\mathrm{recycling},p} \tag{10}$$

Here, $\mathrm{GWP}^S{}_{avoided,p}$ represents the reference-case environmental credit associated with avoided primary-material production, and $\mathrm{GWP}^S{}_{recycling,p}$ represents the corresponding greenhouse-gas burden of recycling operations. A positive $B^S{}_{\mathrm{GWP},p}$ therefore indicates that the avoided burden exceeds the recycling-related burden under the reference scenario.

The integrated screening was constructed using $B^S{}_{\mathrm{GWP},p}$ as the environmental indicator and the screening thermodynamic efficiency, $\eta_{th,p}{}^{scr}$, defined in Equation (9), as the thermodynamic indicator. Total reference-case energy demand, $E_p{}^S$, was used as an additional process-intensity indicator. Accordingly, the three dimensions of the integrated assessment were defined as follows:

$$X_p = B^S_{\mathrm{GWP},p} \tag{11}$$

$$Y_p = \eta^{scr}_{th,p} \tag{12}$$

$$A_p \propto E^S_p \tag{13}$$

Here, A_p denotes the relative marker size used to represent pathway energy demand.

For comparative visualization, the arithmetic mean values of $B^S{}_{\mathrm{GWP},p}$ and $\eta_{th,p}{}^{scr}$ across the three pathways were used as reference lines. These lines were employed only to distinguish relative screening regions and were not interpreted as sustainability thresholds or criteria for identifying an optimal pathway. The resulting framework was therefore used to visualize environmental–thermodynamic trade-offs among the recycling archetypes rather than to establish an absolute ranking of recycling technologies.

2.5. Infrastructure and Decision-Support Scenario Analysis

Because collection distances, transportation costs, spatial waste distribution, and facility locations are not explicitly modeled, the analysis represents preliminary infrastructure screening rather than complete infrastructure optimization or planning.

To extend the process-level screening to recycling-infrastructure planning, three scenario dimensions were considered: future EoL PV waste generation, recycling-facility scale, and electricity decarbonization. These analyses were intended to explore the implications of changing system conditions rather than to predict the performance of a specific future recycling network.

The recycling capacity associated with the projected EoL PV waste stream was calculated as follows:

$$C_{\mathrm{req},y} = r_{\mathrm{rec}} W_y \tag{14}$$

Here, W_y denotes the prescribed EoL PV waste-generation scenario, $C_{\mathrm{req},\underline{y}}$ is the corresponding recycling treatment requirement, and r_{rec} is the assumed recycling fraction. The waste-generation values were adopted as illustrative scenario inputs rather than directly reproduced from the Korea-specific projections cited in Section 3.4. The reference recycling fraction of 0.80 was selected for scenario exploration, with alternative values of 0.60 and 1.00 considered in the sensitivity assessment (Supplementary Table S2).

Facility-scale effects were examined using normalized unit-cost and thermodynamic-intensity indices. A processing capacity of 10 kt yr^{-1} was used as the reference condition, with both indices normalized to unity:

$$C_{\mathrm{rel}} = \frac{C_{\mathrm{unit}}}{C_{\mathrm{unit,ref}}} \tag{15}$$

$$I_{\mathrm{rel}} = \frac{I_{\mathrm{th}}}{I_{\mathrm{th,ref}}} \tag{16}$$

The normalized cost and thermodynamic-intensity values at the six facility capacities were prescribed as discrete scenario inputs rather than generated from an empirically fitted scale-up model (Supplementary Table S2). Connecting lines were used only for visualization. To examine sensitivity to the assumed scale benefits, an alternative scenario was evaluated using $Z(Q;k) = 1 - k\,[1 - Z_{\mathrm{ref}}(Q)]$. Here, Z represents the normalized index, and k = 0, 0.5, and 1.0 denote no, half, and full realization of the prescribed scale benefits, respectively.

Finally, a two-dimensional decision-support space was constructed using normalized waste throughput and electricity-decarbonization level as scenario variables. The decision regions represent alternative combinations of system conditions under which the relative relevance of MR-, CR-, and TR-oriented processing strategies can be explored. The pathway regions and their boundaries were drawn schematically to illustrate possible decision contexts; no empirical transition criteria, optimization, or statistical classification were used to determine these boundaries. Accordingly, the decision space is intended to visualize the sensitivity of pathway selection to future infrastructure and energy-system conditions, rather than to prescribe an optimal recycling technology.

2.6. Scenario Sensitivity Analysis

A sensitivity analysis was performed to evaluate the dependence of the thermodynamic screening results on the scenario-based irreversibility coefficients defined in Table 2. The reference coefficients were varied uniformly by ±10% and ±20% according to the following:

$$\varphi^{S}_{p,i}{}' = \varphi^{S}_{p,i}(1 + \delta) \tag{17}$$

Here, δ was set to −0.20, −0.10, 0, +0.10, and +0.20. For each scenario, the stage-wise and pathway-level screening irreversibility indicators were recalculated using Equations (7) and (8), followed by recalculation of the screening thermodynamic efficiency using Equation (9).

In addition to the uniform coefficient variations, a one-at-a-time sensitivity analysis was performed by independently varying each stage-specific irreversibility coefficient by ±20%, while holding all remaining coefficients at their reference values. The resulting absolute percentage-point changes in screening thermodynamic efficiency were used to quantify the sensitivity magnitude of individual process stages.

The sensitivity analysis was used to examine whether the relative thermodynamic behavior of the three pathway archetypes remained consistent under alternative irreversibility assumptions. Because the variations represent prescribed changes in scenario parameters rather than statistically characterized uncertainties, the resulting ranges are interpreted

as scenario-sensitivity intervals rather than statistical confidence intervals. Probabilistic uncertainty propagation was not performed because defensible probability distributions and correlations for the heterogeneous process inputs and scenario-based coefficients are unavailable.

3. Results and Discussion

3.1. Reference-Case Energy Characteristics of Recycling Pathways

Figure 2 presents the stage-wise energy-demand profiles of the mechanical recycling (MR), chemical recycling (CR), and thermal recycling (TR) pathways under the reference screening scenario defined in Table 2. The total reference-case energy demands were 1.72 kWh panel^{-1} for MR, 4.30 kWh panel^{-1} for CR, and 6.77 kWh panel^{-1} for TR. Accordingly, the scenario-based energy requirement increased in the order MR < CR < TR, with CR requiring approximately 2.5 times and TR approximately 3.9 times the energy assigned to the MR reference case. These values are fixed inputs of the reference screening scenario rather than measured industrial energy demands. Their reported numerical precision is intended for computational reproducibility and does not imply experimentally established accuracy or uncertainty bounds.

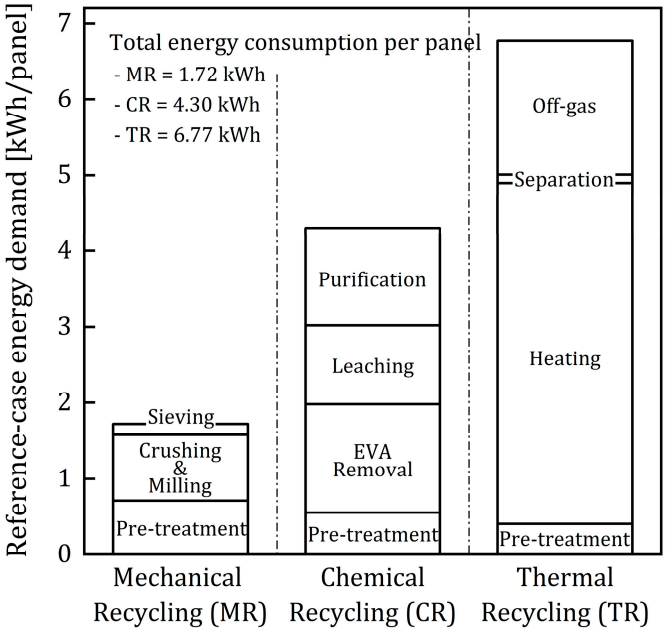


Figure 2. Stage-wise reference-case energy-demand profiles for mechanical (MR), chemical (CR), and thermal (TR) recycling pathways of EoL c-Si PV modules.

The MR pathway exhibited the lowest reference-case energy demand. Crushing and milling accounted for 0.87 kWh panel^{-1}, corresponding to 50.6% of the total MR energy input, followed by pre-treatment at 0.71 kWh panel^{-1} (41.3%) and sieving/separation at 0.14 kWh panel^{-1} (8.1%). The concentration of energy demand in mechanical pre-treatment and material-liberation operations is consistent with the literature evidence summarized in Table 1. In the pilot-scale mechanical process reported by Del Pero et al. (2019), the total electricity requirement was 96.0 kWh t^{-1}, with pre-treatment and subsequent glass, silicon, and Cu/polymer separation accounting for the documented process electricity demand [15]. The reference-case MR value should not be interpreted as a direct reproduction of this pilot process because the stage definitions differ; nevertheless, the literature inventory supports the identification of physical liberation and separation as major energy-demanding functions within mechanical recycling.

The CR pathway exhibited an intermediate reference-case energy demand of 4.30 kWh panel^{-1}. EVA removal was the largest individual contribution at 1.43 kWh panel^{-1} (33.3%), followed by purification at 1.28 kWh panel^{-1} (29.8%), leaching at 1.04 kWh panel^{-1} (24.2%), and pre-treatment at 0.55 kWh panel^{-1} (12.8%). The resulting profile reflects the multi-stage character of chemical recycling, in which delamination is followed by chemical recovery and purification. Literature evidence supports the importance of these operations but also demonstrates substantial heterogeneity in process conditions. Solvent-assisted EVA delamination has been investigated using ultrasonic irradiation and organic solvents, while Pagnanelli et al. (2019) reported cyclohexane-assisted delamination following mechanical pre-treatment [9], and Dias et al. (2016) investigated nitric-acid leaching for Ag recovery [12]. Because these studies employ different functional units and process boundaries, their reported values were used to calibrate the interpretation of the CR archetype rather than to construct an artificially complete pathway inventory.

The TR pathway showed the highest reference-case energy demand, at 6.77 kWh panel^{-1}. Heating and EVA decomposition contributed 4.50 kWh panel^{-1}, equivalent to 66.5% of the total, while off-gas treatment contributed 1.76 kWh panel^{-1} (26.0%). Pre-treatment and post-thermal separation accounted for the remaining 5.9% and 1.6%, respectively. The dominance of thermal treatment is physically consistent with the elevated temperatures required for polymer decomposition. The literature evidence further demonstrates that thermal-processing conditions strongly influence treatment intensity: Dobra et al. (2022) reported that increasing the treatment temperature from 500 to 600 °C reduced the required delamination time from 65 to 33 min, while prior backsheet removal substantially shortened the treatment duration [10]. Fiandra et al. (2019) similarly demonstrated polymer removal and material separation under oxidative thermal treatment at 500 °C [2]. These findings indicate that the energy implications of TR depend not only on the amount of supplied energy but also on temperature, residence time, and the degree of mechanical pre-treatment.

The reference-case comparison therefore identifies distinct energy-demand hotspots for the three pathway archetypes: mechanical liberation in MR, delamination and downstream chemical processing in CR, and high-temperature polymer decomposition in TR. Importantly, the absolute differences among the three reference cases should not be interpreted as evidence that one commercial recycling technology inherently consumes a fixed multiple of another. Rather, they provide a common scenario space for examining how different process structures redistribute energy demand. The literature-informed evidence layer in Table 1 provides the empirical context for this interpretation, while Table 2 provides the internally consistent reference scenario required for comparative screening.

The pathway-specific energy-demand patterns can also be interpreted in relation to recent recycling studies. Fiandra et al. (2023) and Ali et al. (2024) emphasized the role of mechanical liberation and separation in PV recycling, consistent with the concentration of reference-case MR energy demand in crushing and milling [6,7]. Ghahremani et al. (2024) reviewed alternative delamination techniques, highlighting the importance of encapsulant-removal conditions in chemical and thermal processing [11]. These studies support the identification of the principal process functions represented in the present screening, although differences in system boundaries and reporting bases prevent direct quantitative validation of the reference-case pathway totals.

Energy demand alone, however, does not describe the assumed thermodynamic degradation associated with individual process stages. The same reference-case energy inputs were therefore evaluated using the scenario-based irreversibility framework defined in Section 2.3 to examine the distribution of thermodynamic screening indicators among the three pathway archetypes.

3.2. Scenario-Based Thermodynamic Screening and Irreversibility Profiles

Figure 3 presents the stage-wise screening irreversibility profiles of the three recycling pathways under the reference scenario. Based on the energy inputs and scenario-based irreversibility coefficients defined in Table 2, the total screening irreversibility indicators were calculated as 0.89 kWh-eq panel^{-1} for MR, 2.11 kWh-eq panel^{-1} for CR, and 3.17 kWh-eq panel^{-1} for TR. These values represent comparative screening indicators rather than measured exergy destruction in industrial recycling processes. The results therefore describe how the assumed stage-specific irreversibility is distributed within the common reference scenario.

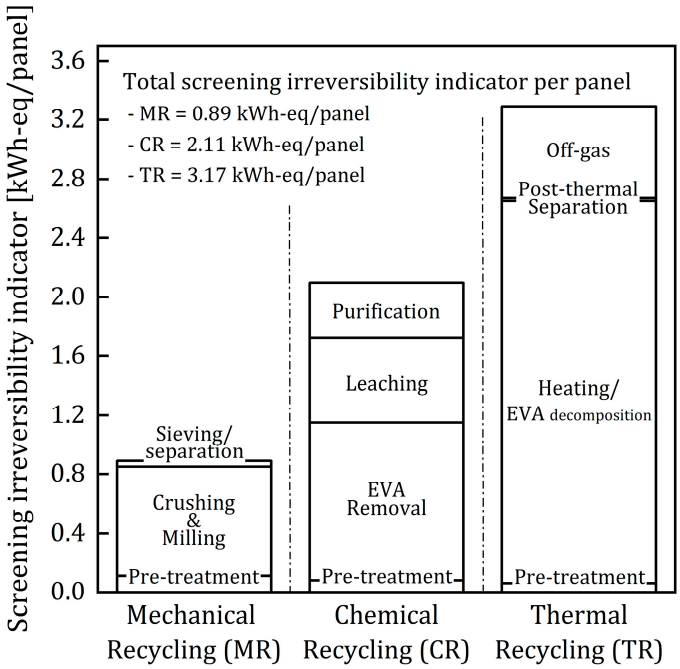


Figure 3. Stage-wise screening irreversibility profiles of mechanical (MR), chemical (CR), and thermal (TR) recycling pathways under the reference scenario.

For MR, crushing and milling dominated the screening irreversibility profile, contributing 0.74 kWh-eq panel^{-1}, or approximately 83.3% of the pathway total. Pre-treatment and sieving/separation contributed approximately 12.0% and 4.7%, respectively. The concentration of the indicator in the comminution stage results from the combination of its relatively large reference-case energy input and the high scenario-based irreversibility coefficient assigned to mechanical size reduction. This result identifies crushing and milling as the principal thermodynamic hotspot within the reference screening scenario, rather than demonstrating a measured second-law loss for an industrial MR process.

The CR pathway exhibited a more distributed profile. EVA removal produced the largest contribution, at 1.07 kWh-eq panel^{-1}, corresponding to approximately 50.8% of the pathway total. Leaching and purification accounted for approximately 27.1% and 18.2%, respectively, while pre-treatment contributed 3.9%. The distribution indicates that the thermodynamic screening outcome for CR is governed primarily by the assumed characteristics of solvent-assisted delamination and subsequent chemical-recovery operations. This interpretation is consistent with the multi-stage nature of the CR archetype identified in the literature-informed evidence layer, although the calculated indicator should not be interpreted as a direct measurement of physicochemical irreversibility.

TR showed the largest pathway-level screening irreversibility indicator. Heating and EVA decomposition contributed approximately 2.48 kWh-eq panel^{-1}, representing 78.0% of the total TR value. Off-gas treatment contributed a further 19.4%, whereas pre-treatment

and post-thermal separation together accounted for less than 3%. The strong concentration in the heating stage reflects both the high reference-case energy requirement assigned to thermal decomposition and its corresponding irreversibility coefficient. Literature evidence summarized in Table 1 independently supports the importance of thermal operating conditions: treatment temperature and residence time vary substantially across thermal-delamination conditions. The screening result therefore identifies thermal treatment as the dominant thermodynamic hotspot of the TR reference case without implying that the calculated value represents experimentally measured exergy destruction.

To account for differences in total energy demand among the pathways, the screening thermodynamic efficiency defined in Equation (9) was also evaluated. The resulting values were 48.4% for MR, 50.9% for CR, and 53.1% for TR. The relatively narrow range of these values, compared with the larger differences in total energy demand, illustrates that energy intensity and the scenario-based thermodynamic indicator describe different aspects of the pathway archetypes. The higher screening thermodynamic efficiency of TR, despite its greater energy demand, results from its lower energy-weighted mean irreversibility coefficient (0.469) compared with CR (0.491) and MR (0.516). This reflects the assigned reference-case parameters rather than a demonstrated thermodynamic advantage of TR.

The thermodynamic screening identifies different pathway-specific hotspots: crushing and milling for MR, EVA removal for CR, and heating/EVA decomposition for TR. These hotspots provide targets for subsequent scenario and sensitivity analysis and illustrate the value of complementing energy-demand comparisons with a stage-resolved thermodynamic screening indicator. However, because the analysis is based partly on scenario-defined irreversibility coefficients, pathway interpretation should be combined with environmental performance and sensitivity analysis rather than treated as an absolute thermodynamic ranking.

The literature-informed thermal-treatment data provide an additional energy-quality perspective. Increasing the treatment temperature from 500 to 600 °C reduced the experimentally reported residence time from 65 to 33 min, while the corresponding thermal-exergy factor, calculated as $\psi_Q = 1 - T_0/T$, increased from 0.614 to 0.659. This result illustrates a process trade-off in which higher-temperature heat provides greater thermodynamic work potential while enabling shorter treatment duration. The comparison is used here as an energy-quality indicator and does not represent a complete exergy balance of the thermal recycling process.

The distinction between energy-demand and thermodynamic screening indicators is also relevant to the recent work of Jech et al. (2025), which combined exergy analysis and life-cycle assessment to compare silicon PV recycling processes [17]. Both studies recognize the value of considering thermodynamic and environmental performance together. However, the present study uses scenario-based irreversibility coefficients rather than complete physical and chemical exergy balances. Consequently, the screening thermodynamic efficiencies reported here should not be compared numerically with conventional second-law efficiencies or interpreted as independently validated thermodynamic performance values.

3.3. Integrated Environmental–Thermodynamic Screening

Figure 4 integrates the reference-case environmental and thermodynamic indicators of the three recycling pathway archetypes. Net GWP benefit is represented on the horizontal axis, screening thermodynamic efficiency $\eta_{th}{}^{scr}$ on the vertical axis, and marker size reflects the total reference-case energy demand. This representation enables the environmental, thermodynamic, and energy-demand characteristics of the pathways to be considered

simultaneously while retaining their status as comparative screening indicators rather than plant-specific performance measurements.

Under the reference scenario, MR exhibited the largest net GWP benefit, at 21.1 kg CO_2-eq panel^{-1}, together with the lowest energy demand of 1.72 kWh panel^{-1}. Its screening thermodynamic efficiency, however, was the lowest of the three pathways at 48.4%. This combination places MR toward the high-environmental-benefit and lower-thermodynamic-screening-efficiency region of the map. The result illustrates an important distinction between energy demand and the thermodynamic screening metric: a pathway characterized by relatively low total energy input does not necessarily exhibit a correspondingly high value of $\eta_{th}{}^{scr}$. For MR, this behavior is primarily associated with the relatively large contribution of crushing and milling to the screening irreversibility indicator identified in Section 3.2.

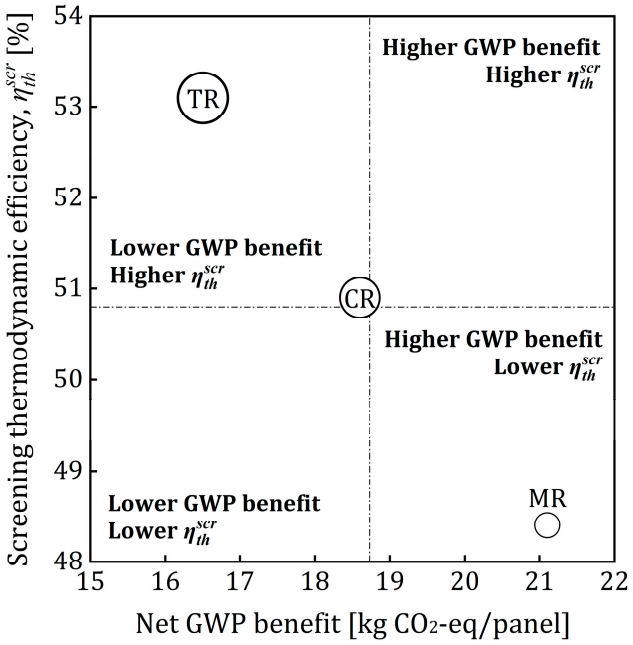


Figure 4. Illustrative environmental–thermodynamic screening of mechanical (MR), chemical (CR), and thermal (TR) recycling pathways under the assumed reference scenario. The reference lines represent arithmetic means of the three scenario points rather than validated sustainability thresholds.

CR occupied an intermediate position in the integrated screening space. Its reference-case net GWP benefit was 18.6 kg CO_2-eq panel^{-1}, while its screening thermodynamic efficiency was 50.9% and its total energy demand was 4.30 kWh panel^{-1}. Compared with MR, the CR reference case therefore combines a lower environmental benefit with a higher thermodynamic screening efficiency and greater energy demand. This intermediate position reflects the multi-stage nature of the CR archetype, in which solvent-assisted delamination, leaching, and purification introduce additional process requirements while enabling material-recovery functions that are not represented by mechanical liberation alone. The result should therefore be interpreted as a trade-off among the selected screening dimensions rather than as evidence that CR is intrinsically superior or inferior to MR.

TR exhibited the highest screening thermodynamic efficiency, at 53.1%, but also the highest reference-case energy demand, at 6.77 kWh panel^{-1}, and the lowest net GWP benefit among the three reference cases, at 16.5 kg CO_2-eq panel^{-1}. Its position therefore differs substantially from that of MR: the TR scenario is characterized by higher thermodynamic screening efficiency but greater process-energy intensity and lower environmental benefit under the adopted assumptions. As discussed in Section 3.2, heating/EVA decomposition

dominates the TR irreversibility profile, while the literature evidence summarized in Table 1 indicates that thermal-treatment requirements are strongly dependent on temperature, residence time, and mechanical pre-treatment. Consequently, the position of TR in the integrated screening space should be interpreted in relation to the assumed process and energy-system conditions rather than as a fixed characteristic of thermal recycling.

The three pathway positions demonstrate that the environmental and thermodynamic screening indicators do not vary in parallel. Increasing screening thermodynamic efficiency from MR to TR is accompanied, under the reference scenario, by increasing energy demand and decreasing net GWP benefit. Thus, none of the pathway archetypes simultaneously exhibits the highest environmental benefit, highest screening thermodynamic efficiency, and lowest energy demand. This trade-off supports the use of multiple indicators for pathway assessment rather than relying on a single energy, environmental, or thermodynamic metric.

For visualization, the arithmetic mean values of the net GWP benefit and screening thermodynamic efficiency were used as reference lines. These correspond to approximately 18.7 kg CO_2-eq panel^{-1} and 50.8%, respectively. The resulting quadrants are intended only to describe the relative positions of the three reference cases and should not be interpreted as absolute sustainability thresholds. In particular, placement of a pathway above or below either reference line does not establish its overall environmental superiority, technological suitability, or industrial feasibility.

The integrated screening therefore provides a compact representation of the trade-offs among the three recycling archetypes. Recent prospective life-cycle assessment of PV recycling systems has likewise emphasized the importance of evaluating recycling configurations in relation to their environmental consequences [20]. More importantly, the relative positions shown in Figure 4 are conditional on the reference-case assumptions adopted in the present framework. Pathway suitability may change with waste throughput, facility scale, electricity-carbon intensity, material-recovery objectives, and other system-level conditions. These dependencies motivate the subsequent infrastructure and decision-support scenario analyses. This conditional interpretation is consistent with previous environmental assessments, including Maani et al. (2020) and Ansanelli et al. (2021), which highlighted the dependence of recycling-related environmental outcomes on process configurations, material recovery, and associated energy or chemical requirements [14,16].

3.4. Future Recycling Demand and Facility-Scale Implications

The process-level results indicate that the implications of EoL PV recycling cannot be evaluated independently of the scale at which future recycling infrastructure is deployed. Figure 5 extends the analysis to the infrastructure level by comparing the adopted EoL PV waste-generation scenario with the corresponding recycling capacity required under the reference recycling fraction of 80%.

Under the adopted scenario, EoL PV waste generation increases from 87.1 kt in 2030 to 267.3 kt in 2035, followed by a more pronounced increase to 820.0 kt in 2040, 1204.9 kt in 2045, and 1771.0 kt in 2050. Application of the 80% recycling fraction defined in Section 2.5 results in corresponding required recycling capacities of approximately 69.7, 213.8, 656.0, 963.9, and 1416.8 kt, respectively. Thus, the scenario represents an approximately twenty-fold increase in both EoL PV waste generation and associated recycling-capacity requirements between 2030 and 2050. The direction of this scenario is consistent with recent Korea-specific studies reporting a substantial increase in retired PV modules as earlier installation cohorts reach end of life [21,22].

These values should be interpreted as scenario-based infrastructure requirements rather than forecasts of actual installed recycling capacity. Nevertheless, the magnitude

of the increase illustrates an important planning issue: recycling systems designed for relatively limited near-term waste volumes may need to accommodate substantially greater material throughput as larger cohorts of installed PV modules reach end of life. Infrastructure planning therefore involves not only the choice of recycling process but also the timing and scale at which treatment capacity becomes available. For 2050, changing the assumed recycling fraction from 0.60 to 1.00 changes the corresponding treatment requirement from 1062.6 to 1771.0 kt, compared with 1416.8 kt under the reference fraction of 0.80 (Supplementary Table S2).

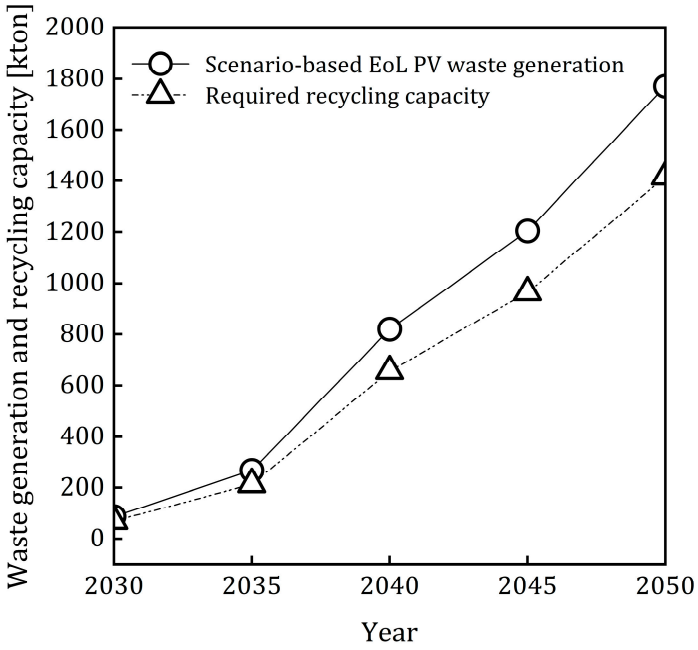


Figure 5. Scenario-based EoL PV waste generation and corresponding recycling-capacity requirement in South Korea from 2030 to 2050.

The facility-scale scenario in Figure 6 examines this issue using normalized unit-cost and thermodynamic-intensity indices. At the reference processing capacity of 10 kt yr^{-1}, both indices were normalized to 1.00. As capacity increases to 30, 50, 100, 200, and 300 kt yr^{-1}, the relative unit-cost index decreases to 0.78, 0.70, 0.62, 0.58, and 0.56, respectively. Over the same capacity range, the relative thermodynamic-intensity index decreases to 0.88, 0.82, 0.76, 0.72, and 0.70. The scenario therefore corresponds to reductions of approximately 44% in relative unit cost and 30% in relative thermodynamic intensity between the 10 and 300 kt yr^{-1} reference conditions.

Importantly, the trajectories in Figure 6 are normalized screening scenarios rather than empirically fitted scale-up relationships for commercial PV recycling facilities. Although previous studies have emphasized the importance of processing scale and facility configuration in PV recycling [3,9,15], directly comparable empirical ranges for the normalized indices adopted here are not available. Therefore, the assumed trajectories should not be interpreted as quantitatively validated scale-up relationships. They are intended to examine how potential scale effects could influence infrastructure decisions if increasing throughput enables improved equipment utilization, process integration, and distribution of fixed operational requirements. Accordingly, the numerical reductions should not be interpreted as predictions that a 300 kt yr^{-1} facility will necessarily achieve the indicated cost or thermodynamic performance. At 300 kt yr^{-1}, assuming only half of the reference scale benefit increases the relative unit-cost and thermodynamic-intensity indices from

0.56 and 0.70 to 0.78 and 0.85, respectively, illustrating their dependence on the prescribed scale-effect assumptions (Supplementary Table S2).

The combined interpretation of Figures 5 and 6 illustrates the connection between process assessment and infrastructure planning. Increasing EoL PV waste volumes can create conditions in which larger processing capacities become relevant, while potential scale effects may alter the relative importance of process energy, cost, and thermodynamic intensity. However, larger facilities are not necessarily preferable in all circumstances. Increased centralization may also increase collection distances, transportation requirements, regional dependence on waste supply, and the risk of underutilized capacity when feedstock availability is insufficient. Conversely, smaller or modular facilities may offer greater flexibility where waste generation is spatially dispersed or uncertain.

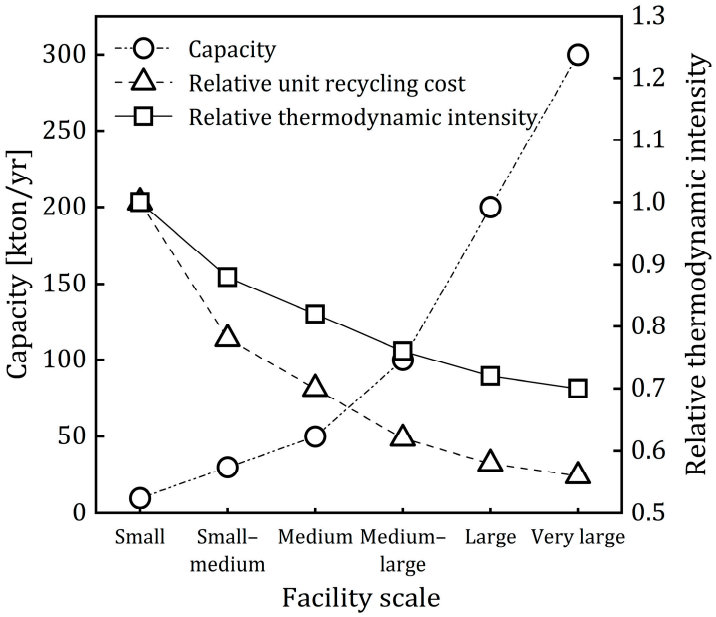


Figure 6. Scenario-based facility-scale trajectories for normalized unit recycling cost and thermodynamic intensity.

Consequently, facility scale should be regarded as a decision variable rather than a predetermined optimization outcome. The appropriate configuration depends on the interaction among waste availability, processing technology, logistics, energy supply, and infrastructure timing. This infrastructure perspective complements the process-level screening in Sections 3.1–3.3 and provides the basis for examining how pathway relevance may change under alternative waste-throughput and electricity-decarbonization conditions.

3.5. Pathway Decision-Support Scenarios and Sensitivity Analysis

Figure 7 extends the process- and infrastructure-level results into a two-dimensional decision-support space defined by waste throughput and electricity decarbonization. The map is intended to illustrate how the relative relevance of MR-, CR-, and TR-oriented recycling strategies may shift as system conditions change. The boundaries between the regions represent conceptual screening boundaries rather than empirically determined technological thresholds or optimization results.

At relatively low waste throughput, the MR-oriented region reflects the comparatively low reference-case energy requirement and simpler process structure identified in the process-level screening. As throughput increases, the relevance of more intensive chemical or combined processing configurations may increase, represented by the intermediate CR-oriented region. At higher throughput and greater electricity decarbonization, the scenario

space extends toward the TR-oriented region, where the greater energy requirement of thermal processing may become less restrictive from an electricity-related environmental perspective. These regions should not be interpreted as demonstrating that a particular pathway is universally preferable under the corresponding conditions. Rather, they illustrate how infrastructure scale and energy-system conditions can modify the context in which the process-level trade-offs identified in Sections 3.1–3.4 are evaluated.

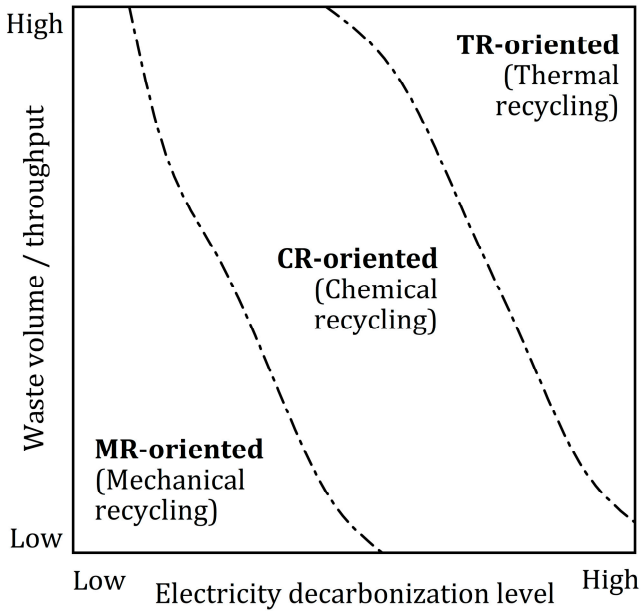


Figure 7. Conceptual decision-support illustration of MR-, CR-, and TR-oriented recycling strategies under varying waste-throughput and electricity-decarbonization conditions. The schematic boundaries are not empirically estimated or optimized transition thresholds.

This interpretation is particularly important because practical recycling systems may combine operations from more than one pathway. Mechanical pre-treatment can precede chemical or thermal delamination, and the appropriate configuration may depend on material-recovery objectives, available throughput, regional logistics, energy supply, and facility utilization. Figure 7 therefore serves as a scenario-based decision-support representation linking process characteristics to infrastructure-planning conditions rather than as a prescriptive technology-selection map.

The sensitivity of the thermodynamic screening results to the assumed irreversibility coefficients was additionally evaluated by varying all reference φ^S values by ±10% and ±20%, as defined in Section 2.6. Table 3 summarizes the resulting screening thermodynamic efficiencies. Under a 20% reduction in the irreversibility coefficients, ${\eta_{th}}^{scr}$ increased to 58.7%, 60.7%, and 62.5% for MR, CR, and TR, respectively. Under a 20% increase, the corresponding values decreased to 38.0%, 41.1%, and 43.8%. The intermediate ±10% scenarios produced corresponding changes between these limits.

The sensitivity results show that the absolute values of the screening thermodynamic efficiency depend appreciably on the assumed irreversibility coefficients, as expected from the formulation of the screening model. However, the relative ordering of the three reference pathway archetypes remains unchanged over the investigated ±20% range. This indicates that the comparative pattern obtained under the reference scenario is not reversed by moderate uniform variation of φ^S.

This result should not be interpreted as statistical validation of the thermodynamic model. The investigated ranges represent prescribed scenario variations rather than probability-based uncertainty intervals, and the stability of the relative ordering does

not demonstrate that the underlying coefficients represent measured industrial irreversibility. Instead, the sensitivity analysis indicates that the principal comparative pattern of the reference screening is maintained within the specified scenario range.

Table 3. Scenario sensitivity of screening thermodynamic efficiency to variations in the irreversibility coefficients.

Scenario	φ^S Multiplier	MR $\eta_{th}{}^{scr}$ [%]	CR $\eta_{th}{}^{scr}$ [%]	TR $\eta_{th}{}^{scr}$ [%]
Low-irreversibility scenario	−20%	58.7	60.7	62.5
Moderate-low scenario	−10%	53.5	55.8	57.8
Reference case	0%	48.4	50.9	53.1
Moderate-high scenario	+10%	43.2	46.0	48.4
High-irreversibility scenario	+20%	38.0	41.1	43.8

To further examine the influence of individual process assumptions, an independent stage-wise sensitivity analysis was conducted by varying each irreversibility coefficient by ±20%, while keeping all other coefficients at their reference values (Figure 8). The largest changes in screening thermodynamic efficiency were observed for crushing and milling in MR (±8.60 percentage points), heating/EVA decomposition in TR (±7.31 percentage points), and EVA removal in CR (±4.99 percentage points). For example, reducing only the MR crushing/milling coefficient by 20% increases its screening efficiency to 56.97%, exceeding the TR reference value of 53.13%, demonstrating that the pathway ranking can be reversed by independent coefficient variations. These results indicate that the sensitivity of the screening indicators is concentrated in a limited number of energy-intensive stages. Unlike the uniform sensitivity analysis summarized in Table 3, the stage-wise analysis identifies the relative influence of individual coefficients, although the resulting variations remain prescribed scenarios rather than statistically quantified uncertainty.

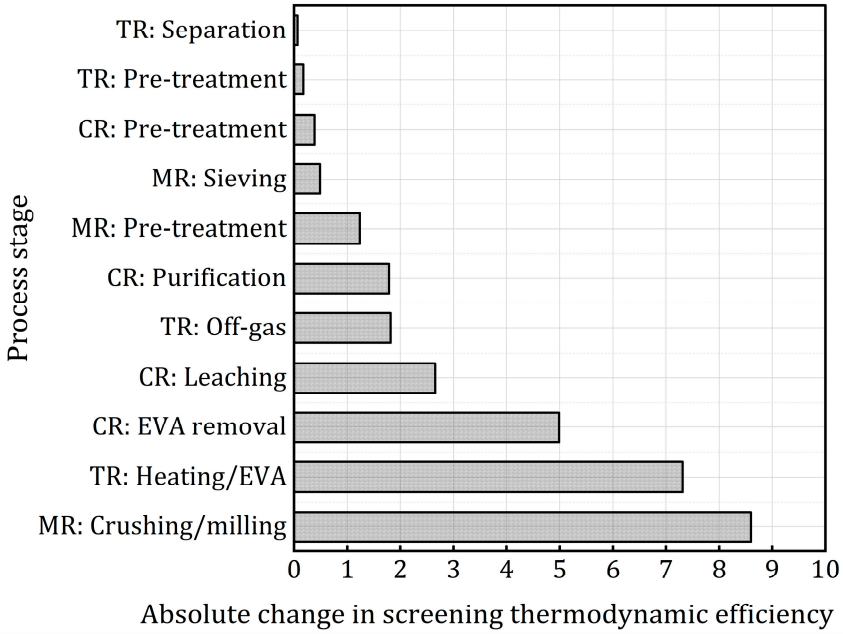


Figure 8. Independent stage-wise sensitivity of screening thermodynamic efficiency to ±20% variations in individual scenario-based irreversibility coefficients. Each bar represents the absolute percentage-point change from the reference case, with all other coefficients held constant.

The sensitivity results should be interpreted in relation to the available literature rather than as directly validated thermodynamic performance ranges. Previous studies have identified mechanical liberation, solvent-assisted delamination, and thermal treatment as important operations in PV recycling [10,11,15]. These observations are qualitatively consistent with the stages exhibiting the greatest sensitivity in Figure 8. However, the reported sensitivity magnitudes are derived from prescribed variations in scenario-based irreversibility coefficients, for which directly comparable experimental ranges are not available. Consequently, the results demonstrate the relative influence of the assumed process parameters within the present screening framework rather than quantitative agreement with measured industrial exergy performance.

Taken together, the decision-support and sensitivity analyses emphasize that recycling-pathway assessment should be conditional on both process characteristics and infrastructure context. The framework therefore does not identify a single optimal recycling pathway; rather, it provides a structured means of examining how pathway relevance may evolve with waste availability, facility scale, energy-system decarbonization, and thermodynamic assumptions. This conditional interpretation forms the basis for using energy, exergy, and environmental screening as an input to longer-term recycling-infrastructure planning. The evidential status of the principal screening findings and decision-support interpretations is summarized in Supplementary Table S1.

4. Conclusions

This study developed an integrated energy, exergy, and environmental screening framework for comparing mechanical recycling (MR), chemical recycling (CR), and thermal recycling (TR) pathways for end-of-life crystalline silicon photovoltaic modules and for examining their implications for recycling-infrastructure planning. By distinguishing the literature-derived evidence, calculated indicators, and scenario-based parameters, the framework provides a comparative assessment without implying the performance of specific commercial recycling facilities.

Under the reference scenario, total energy demands were 1.72, 4.30, and 6.77 kWh panel^{-1} for MR, CR, and TR, respectively, while the corresponding screening irreversibility indicators were 0.89, 2.11, and 3.17 kWh-eq panel^{-1}. The screening thermodynamic efficiencies were 48.4%, 50.9%, and 53.1%, respectively. Distinct process hotspots were identified for each pathway: crushing and milling for MR, EVA removal for CR, and heating/EVA decomposition for TR. Integrated environmental–thermodynamic screening further revealed that energy demand, environmental benefit, and thermodynamic performance do not vary in parallel. MR combined relatively low energy demand with a high reference-case environmental benefit, whereas TR showed higher screening thermodynamic efficiency but greater energy requirements, with CR occupying an intermediate position.

The infrastructure scenarios further indicate that increasing EoL PV waste volumes, facility scale, and electricity decarbonization can alter the context in which recycling pathways are evaluated. Consequently, the framework does not identify a universally superior recycling technology; rather, it highlights waste availability, facility scale, energy-system conditions, and process characteristics as interacting variables for recycling-infrastructure planning and decision support. The thermodynamic and infrastructure results are conditional on the adopted screening assumptions and should not be interpreted as validated industrial-performance predictions, particularly given the incomplete process inventories and scenario-based irreversibility and scale parameters. Future work should therefore prioritize harmonized industrial process inventories, experimentally resolved exergy balances, validated environmental data, and integration with spatial, transportation, and economic models.

Supplementary Materials: The following supporting information can be downloaded at https://www.mdpi.com/article/10.3390/en19215153/s1: Table S1: Evidence classification, provenance, and computational roles of input parameters and derived indicators used in the energy–exergy, environmental, and infrastructure screening framework; Table S2: Sensitivity of recycling treatment requirements and normalized facility-scale indices to prescribed recycling fractions and scale-benefit assumptions.

Author Contributions: Conceptualization, M.Y.K. and S.J.H.; methodology, S.J.H.; software, S.J.H.; validation, M.Y.K. and S.J.H.; formal analysis, S.J.H.; investigation, M.Y.K. and S.J.H.; resources, M.Y.K. and S.J.H.; data curation, S.J.H.; writing—original draft preparation, S.J.H.; writing—review and editing, M.Y.K. and S.J.H.; visualization, S.J.H.; supervision, M.Y.K.; project administration, M.Y.K.; funding acquisition, M.Y.K. All authors have read and agreed to the published version of the manuscript.

Funding: This research was supported by the ANCHOR program through the Jeonbuk Anchor Center, funded by the Ministry of Education (MOE) and the Jeonbuk State, Republic of Korea (2026-ANCHOR-13-JJU).

Data Availability Statement: The principal input classifications, scenario parameters, and sensitivity results are provided in the Supplementary Materials. Additional calculation data supporting the reported screening results are available from the corresponding author upon reasonable request.

Acknowledgments: During the preparation of this manuscript, the authors used OpenAI's ChatGPT (GPT-6) to assist with the numerical-analysis workflows, data processing, and language editing. The authors reviewed and verified all numerical interpretations and manuscript content. The authors take full responsibility for the content of this publication.

Conflicts of Interest: The authors declare no conflicts of interest.

Abbreviations

The following abbreviations are used in this manuscript:

c-Si	Crystalline silicon
CR	Chemical recycling
EoL	End-of-life
EVA	Ethylene-vinyl acetate
GWP	Global warming potential
LCA	Life-cycle assessment
MR	Mechanical recycling
PV	Photovoltaic
TR	Thermal recycling
WEEE	Waste electrical and electronic equipment

References

1. Lunardi, M.M.; Alvarez-Gaitan, J.P.; Bilbao, J.I.; Corkish, R. Comparative life cycle assessment of end-of-life silicon solar photovoltaic modules. *Appl. Sci.* **2018**, *8*, 1396. [CrossRef]
2. Fiandra, V.; Sannino, L.; Andreozzi, C.; Corcelli, F.; Graditi, G. Silicon photovoltaic modules at end-of-life: Removal of polymeric layers and separation of materials. *Waste Manag.* **2019**, *87*, 97–107. [CrossRef] [PubMed]
3. Dias, P.; Schmidt, L.; Lunardi, M.M.; Chang, N.L.; Spier, G.; Corkish, R.; Veit, H. Comprehensive recycling of silicon photovoltaic modules incorporating organic solvent delamination–technical, environmental and economic analyses. *Resour. Conserv. Recycl.* **2021**, *165*, 105241. [CrossRef]
4. Gahlot, R.; Mir, S.; Dhawan, N. Recycling of discarded photovoltaic solar modules for metal recovery: A review and outlook for the future. *Energy Fuels* **2022**, *36*, 14554–14572. [CrossRef]
5. Akimoto, Y.; Iizuka, A.; Shibata, E. High-voltage pulse crushing and physical separation of polycrystalline silicon photovoltaic panels. *Miner. Eng.* **2018**, *125*, 1–9. [CrossRef]

6. Fiandra, V.; Sannino, L.; Andreozzi, C. Photovoltaic waste as source of valuable materials: A new recovery mechanical approach. *J. Clean. Prod.* **2023**, *385*, 135702. [CrossRef]
7. Ali, A.; Shahid, M.; Qadir, S.A.; Islam, T.; Khan, M.W.; Ahmed, S. Solar PV end-of-life waste recycling: An assessment of mechanical recycling methods and proposed hybrid laser and high voltage pulse crushing method. *Resources* **2024**, *13*, 169. [CrossRef]
8. Kim, Y.; Lee, J. Dissolution of ethylene vinyl acetate in crystalline silicon PV modules using ultrasonic irradiation and organic solvent. *Sol. Energy Mater. Sol. Cells* **2012**, *98*, 317–322. [CrossRef]
9. Pagnanelli, F.; Moscardini, E.; Altimari, P.; Padoan, F.C.; Atia, T.A.; Beolchini, F.; Amato, A.; Toro, L. Solvent versus thermal treatment for glass recovery from end of life photovoltaic panels: Environmental and economic assessment. *J. Environ. Manag.* **2019**, *248*, 109313. [CrossRef] [PubMed]
10. Dobra, T.; Vollprecht, D.; Pomberger, R. Thermal delamination of end-of-life crystalline silicon photovoltaic modules. *Waste Manag. Res.* **2022**, *40*, 96–103. [CrossRef] [PubMed]
11. Ghahremani, A.; Adams, S.D.; Norton, M.; Khoo, S.Y.; Kouzani, A.Z. Delamination techniques of waste solar panels: A review. *Clean Technol.* **2024**, *6*, 280–298. [CrossRef]
12. Dias, P.; Javimczik, S.; Benevit, M.; Veit, H.; Bernardes, A.M. Recycling WEEE: Extraction and concentration of silver from waste crystalline silicon photovoltaic modules. *Waste Manag.* **2016**, *57*, 220–225. [CrossRef] [PubMed]
13. Rubino, A.; Granata, G.; Moscardini, E.; Baldassari, L.; Altimari, P.; Toro, L.; Pagnanelli, F. Development and techno-economic analysis of an advanced recycling process for photovoltaic panels enabling polymer separation and recovery of Ag and Si. *Energies* **2020**, *13*, 6690. [CrossRef]
14. Maani, T.; Celik, I.; Heben, M.J.; Ellingson, R.J.; Apul, D. Environmental impacts of recycling crystalline silicon (c-SI) and cadmium telluride (CDTE) solar panels. *Sci. Total Environ.* **2020**, *735*, 138827. [CrossRef] [PubMed]
15. Del Pero, F.; Delogu, M.; Berzi, L.; Escamilla, M. Innovative device for mechanical treatment of End of Life photovoltaic panels: Technical and environmental analysis. *Waste Manag.* **2019**, *95*, 535–548. [CrossRef] [PubMed]
16. Ansanelli, G.; Fiorentino, G.; Tammaro, M.; Zucaro, A. A life cycle assessment of a recovery process from end-of-life photovoltaic panels. *Appl. Energy* **2021**, *290*, 116727. [CrossRef]
17. Jech, Š.; Bartie, N.; Tas, G.; Miettunen, K.; Serna-Guerrero, R.; Santasalo-Aarnio, A. Beyond material recovery: Exergy and environmental analysis of silicon solar panel recycling. *Sol. Energy Mater. Sol. Cells* **2025**, *286*, 113561. [CrossRef]
18. Diez-Suarez, A.-M.; Martínez-Benavides, M.; Donado, C.M.; Blanes-Peiró, J.-J.; Torres, E.J.M. Recycling of silicon-based photovoltaic modules: Mediterranean region insight. *Energies* **2024**, *17*, 6015. [CrossRef]
19. Cheema, H.A.; Ilyas, S.; Kang, H.; Kim, H. Comprehensive review of the global trends and future perspectives for recycling of decommissioned photovoltaic panels. *Waste Manag.* **2024**, *174*, 187–202. [CrossRef] [PubMed]
20. Heiho, A.; Suwa, I.; Dou, Y.; Lim, S.; Namihira, T.; Koita, T.; Mochidzuki, K.; Murakami, S.; Daigo, I.; Tokoro, C.; et al. Prospective life cycle assessment of recycling systems for spent photovoltaic panels by combined application of physical separation technologies. *Resour. Conserv. Recycl.* **2023**, *192*, 106922. [CrossRef]
21. Lee, S.-H.; Jang, Y.-C. Analysis for End-of-Life Solar Panel Generations by Renewable Energy Supply towards Carbon Neutrality in South Korea. *Energies* **2023**, *16*, 8039. [CrossRef]
22. Kwon, S.; Kim, H.J.; Kim, S.; Hong, S.J. Sustainability impact evaluation of the recycling of end-of-life crystalline silicon solar photovoltaic panel waste in South Korea. *Sustainability* **2025**, *17*, 431. [CrossRef]

Disclaimer/Publisher's Note: The statements, opinions and data contained in all publications are solely those of the individual author(s) and contributor(s) and not of MDPI and/or the editor(s). MDPI and/or the editor(s) disclaim responsibility for any injury to people or property resulting from any ideas, methods, instructions or products referred to in the content.